# Optical characterization of poly-$SiO_x$ and poly-$SiC_x$ carrier-selective passivating contacts

Singh, M.; Santbergen, R.; Mazzarella, L.; Madrampazakis, A.; Yang, G.; Vismara, R.; Remes, Z.; Weeber, A.; Zeman, M.; Isabella, O.

**DOI**
10.1016/j.solmat.2020.110507

**Publication date**
2020

**Document Version**
Final published version

**Published in**
Solar Energy Materials and Solar Cells

Solar Energy Materials & Solar Cells 210 (2020) 110507

Contents lists available at ScienceDirect

Solar Energy Materials and Solar Cells

journal homepage: http://www.elsevier.com/locate/solmat

# Optical characterization of poly-$SiO_x$ and poly-$SiC_x$ carrier-selective passivating contacts

M. Singh [a,*], R. Santbergen [a], L. Mazzarella [a], A. Madrampazakis [a], G. Yang [a], R. Vismara [a], Z. Remes [b], A. Weeber [a,c], M. Zeman [a], O. Isabella [a]

[a] Delft University of Technology, PVMD Group, Mekelweg 4, 2628 CD, Delft, the Netherlands
[b] Institute of Physics AS CR, Vvi, Cukrovarnická 10/112, 162 00, Prague 6, Czech Republic
[c] ECN Part of TNO, Solar Energy, PO Box 15, 1755 ZG, Petten, the Netherlands

ARTICLE INFO

*Keywords:*
Carrier-selective passivating contacts
Absorption coefficients
Photothermal deflection spectroscopy
Reflection-transmission
Poly-$SiO_x$
Poly-$SiC_x$

ABSTRACT

The optical modelling for optimizing high-efficiency c-Si solar cells endowed with poly-$SiO_x$ or poly-$SiC_x$ carrier-selective passivating contacts (CSPCs) demands a thorough understanding of their optical properties, especially their absorption coefficient. Due to the mixed phase nature of these CSPCs, spectroscopic ellipsometry is unable to accurately detect the weak free carrier absorption (FCA) at long wavelengths. In this work, the absorption coefficient of doped poly-$SiO_x$ and poly-$SiC_x$ layers as function of oxygen and carbon content, respectively, was obtained for wavelengths (300–2000 nm) by means of two alternative techniques. The first approach, photothermal deflection spectroscopy (PDS), was used for layers grown on quartz substrates and is appealing from the point of view of sample fabrication. The second, a novel inverse modelling (IM) approach based on reflectance and transmittance measurements, was instead used for layers grown on textured c-Si wafer substrates to mimic symmetrical samples. Although the absorption coefficients obtained from these two techniques slightly differ due to the different used substrates, we could successfully measure weak FCA in our CSPCs layers. Using an in-house developed multi-optical regime simulator and comparing modelled reflectance and transmittance with measured counterparts from symmetrical samples, we confirmed that with increasing doping concentration FCA increases; and found that the absorption coefficients obtained from IM can now be used to perform optical simulations of these CSPCs in solar cells.

## 1. Introduction

Polycrystalline silicon (poly-Si) has proven to be a dominating candidate in the field of carrier-selective passivating contacts (CSPCs) [1–4]. However, doped poly-Si suffers from high free carrier absorption (FCA), which has turned the attention of the researchers towards new wide bandgap materials, such as polycrystalline silicon oxide (poly-$SiO_x$) and polycrystalline silicon carbide (poly-$SiC_x$). In these materials, the optoelectronic properties depend on oxygen [5] and carbon [6] content. Poly-$SiO_x$ layers are promising candidates as CSPCs for high-efficiency c-Si solar cells [5,7–9], with implied $V_{OC}$ up to 740 (716) mV for n-type (p-type) doping [5,10] on flat wafer. Symmetric samples of n-type (p-type) poly-$SiC_x$ layers have shown an implied $V_{OC}$ as high as 746 mV (735 mV) [6,11] on flat wafer. To increase the efficiency of front/back-contacted (FBC) and interdigitated back-contacted (IBC) c-Si solar cells endowed with poly-$SiO_x$ or poly-$SiC_x$ CSPCs, opto-electrical modelling can provide guidelines. So far, researchers have mostly focused on structural [9,12] and electrical properties [13,14] of these layers. However, not much extensive research has been done to optically characterize these poly-$SiO_x$ and poly-$SiC_x$ layers. In this respect, it is instrumental to know - in first place - the absorption coefficient (α), because it is a crucial parameter for understanding the optical properties of these mixed phase materials [5,9,14].

The goal of this work is therefore to obtain accurate absorption coefficients of doped poly-$SiO_x$ and poly-$SiC_x$ layers, that can be used for the optical simulations of solar cells with these CSPCs. We first investigate if the substrate affects the absorption coefficients of these CSPCs. Then, we also study the effect of changing oxygen and carbon concentration on the optical properties of our in-house developed poly-$SiO_x$ and poly-$SiC_x$ layers, respectively.

Owing to their non-trivial structural nature, the approach based on spectroscopic ellipsometry (SE) is prone to under-/over-estimation of

* Corresponding author.
*E-mail address:* M.Singh-1@tudelft.nl (M. Singh).

https://doi.org/10.1016/j.solmat.2020.110507
Received 2 October 2019; Received in revised form 5 February 2020; Accepted 9 March 2020
Available online 25 March 2020

the absorption coefficients [5]. Also, weak absorption is difficult to detect using SE [15]. A possible alternative technique could be photothermal deflection spectroscopy (PDS), which has been previously used to directly measure the absolute absorption in thin films and is sensitive to absorption values lower than 1% [16].

We have therefore deployed the absolute PDS technique to measure the absorption coefficient of doped poly-$SiO_x$ and poly-$SiC_x$ layers. For non-absorptive substrates must be used, layers have been deposited on fused silica quartz substrates. However, in solar cells, these CSPCs layers are deposited on (textured) c-Si wafers, for which the optical properties may be different. Thus, for optical simulations of solar cells with these CSPCs layers, it is necessary to investigate if the absorption coefficients obtained from PDS on quartz substrate can be used. Hence, absorption coefficients from PDS are used as an input for optical simulations using GenPro4 [17] to generate reflection ($R$), transmission ($T$) and absorption ($A$) spectra of these highly-transparent CSPCs on flat or textured c-Si wafer substrates.

This two-step process – (i) PDS-based absorption coefficients of flat samples (ii) verified on simulated absorption spectra of (textured) c-Si wafers – may not always give an accurate fit. Therefore, we have used also another method, the so-called inverse modelling (IM). This method allows to derive absorption coefficients directly from reflectance/transmittance (RT) measurements of symmetric c-Si samples coated both sides with CSPCs. As RT measurements typically have an accuracy of 1%, this method is usually not sensitive enough for weakly absorbing films, for instance layers that absorb less than 1% of the incident light. Rudiger et al. increase the sensitivity of the RT measurements by utilizing textured c-Si wafers in which weakly-absorbed light can be efficiently trapped. This enhances the path length up to a factor of 50, resulting in a significant absorption enhancement [18]. Therefore, the cumulative multi-pass absorption can be detected using conventional RT measurements, even when the single-pass absorption is much less than 1% [19]. However, Rudiger et al. used a silver (Ag) back reflector, whose optical properties depend on the deposition conditions [20]. The drawback of including an Ag back reflector is that in optical simulations, when Ag has slightly different optical properties compared to the ones used in simulations, it might attribute too little absorptance to Ag and too much to the layer under test, or vice versa. We improve this method by considering symmetrical samples without metal back reflector. This eliminates the need to account for absorption in the metal and the corresponding errors that this might introduce. Rudiger et al. use this method to measure the FCA in doped regions inside the c-Si wafer. In our RT measurements, for photon energies lower than that of c-Si bandgap and knowing wafer's resistivity (i.e. the base doping concentration), we can attribute the absorption mainly to the investigated CSPCs thin film. Then, if the film thickness is known, we hereby show that the corresponding absorption coefficients can be obtained through IM. The absorption coefficients obtained from PDS measurements have been obviously compared to those obtained from IM and found differences will be discussed here.

## 2. Experiments and methods

### 2.1. Sample preparation

To prepare flat n type doped poly-$SiO_x$ layers, suitable for certain optical measurements, hydrogenated amorphous silicon oxide (a-$SiO_x$:H) was deposited using plasma enhanced chemical vapour deposition (PECVD) technique on fused silica substrates. The sample structure is shown in Fig. 1a. A combination of gases such as carbon dioxide ($CO_2$), molecular hydrogen ($H_2$), silane ($SiH_4$) was used as basis, while phosphine gas ($PH_3$) was used for n-type doping source. For p-type doped poly-$SiO_x$ layers, diborane gas ($B_2H_6$) was used as p-type doping source. For poly-$SiO_x$ layers, we defined $R_{CO2}$ ratio as:

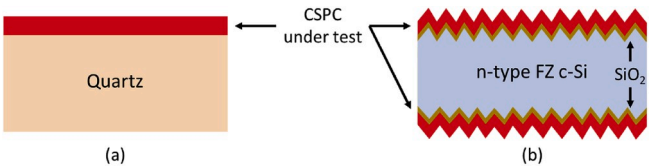


**Fig. 1.** Samples (a) are for PDS, Raman and SE measurements; samples (b) are for RT measurements.

$$R_{CO_2} = \frac{CO_2}{CO_2 + SiH_4} \quad (1)$$

to rank our doped poly-$SiO_x$ layers as function of oxygen content. These layers were annealed at 850 °C for 45 min. After high temperature annealing, these amorphous layers became poly-crystalline with phosphorous doping atoms being activated. Similarly (see Fig. 1a), for n-type doped poly-$SiC_x$ layers, we deposited first hydrogenated amorphous silicon carbide (a-$SiC_x$:H) from $H_2$, $SiH_4$ and methane ($CH_4$) gases as basis and again $PH_3$ for n-type doping source. For p-type doped poly-$SiC_x$ layers, $B_2H_6$ gas was used as p-type doping source. In this case, the ratio $R_{CH4}$ was defined as:

$$R_{CH_4} = \frac{CH_4}{CH_4 + SiH_4} \quad (2)$$

and was used to rank doped poly-$SiC_x$ layers as function of carbon content. These layers were also annealed at 850 °C albeit for a shorter amount of time (5 min) with respect to poly-$SiO_x$ counterparts. Other defined ratios are $R_{PH_3} = \frac{PH_3}{PH_3+SiH_4}$ and $R_{B_2H_6} = \frac{B_2H_6}{B_2H_6+SiH_4}$ to study the effect of varying doping concentration on the optical properties of our layers. The deposition parameters are given in Table 1.

Afterwards, we also prepared n-type and p-type doped poly-$SiO_x$ and poly-$SiC_x$ layers on textured c-Si wafers. Float zone (FZ) double-side polished n-type c-Si wafers (thickness: 280 ± 20 μm, orientation: <100>, resistivity: 1–5 Ω cm) were chemically textured in a solution containing TMAH, AlkaText® surfactant and water to obtain pyramids on both sides. Then, a thin layer of tunnelling $SiO_2$ [1] was wet-chemically grown on both sides by nitric acid oxidation of silicon (NAOS). These substrates were loaded in PECVD equipment to be coated on both sides by n-type or p-type doped a-$SiO_x$:H or a-$SiC_x$:H layers. All samples were annealed at 850 °C for 45 min in case of poly-$SiO_x$ and 5 min in case of poly-$SiC_x$. The structure of these samples is sketched in Fig. 1b.

### 2.2. Characterization methods

Raman measurements were performed using Renishaw's inVia Raman microscope at an excitation wavelength of 514 nm. The equipment was calibrated by measuring sharp peak at 520.5 $cm^{-1}$ on c-Si wafer. SE measurements were performed using a J. A. Woolam ellipsometer to obtain the refractive indices and absorption coefficients of these layers. The absorptance of poly-$SiO_x$ and poly-$SiC_x$ layers were measured using two complementary techniques: PDS and RT. PDS measures the absorption in CSPCs layers on quartz substrate whereas the RT technique measures the absorption in CSPCs layers on (textured) c-Si wafer substrates. PDS measures the deflection of a laser beam passing through a cuvette filled with a suitable liquid (FC72 in our case), due to the heat absorbed by the layer under test immersed in the cuvette. The setup used for PDS measurements is shown in Fig. 2. More details about

**Table 1**
Deposition parameters of n-type doped poly-$SiO_x$ and poly-$SiC_x$ layers.

| Type | $T_{substrate}$ (°C) | $P_{deposition}$ (mbar) | Power density (W/$cm^2$) |
|---|---|---|---|
| poly-$SiO_x$ | 180 | 1 | 0.035 |
| poly-$SiC_x$ | 180 | 0.7 | 0.021 |

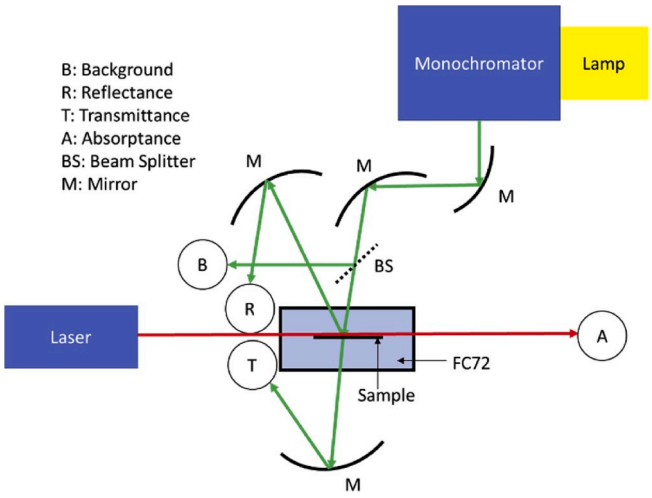


**Fig. 2.** Schematic sketch of the absolute PDS setup used in this work.

this technique can be found elsewhere [16]. For these measurements, we used samples as in Fig. 1a, whose quartz substrate does not contribute to absorption. For obtaining the wavelength-dependent absorption coefficient using the *absolute* PDS method [16], $R_{PDS}$, $T_{PDS}$ and $A_{PDS}$ spectra have been simultaneously measured at the same spot in the wavelength range from 300 nm to 2000 nm. $R_{PDS}$ and $T_{PDS}$ were measured with two independent detectors opportunely placed on the optical Table and coupled with the PDS setup. In Fig. 3, these curves have been plotted for n-type doped poly-$SiO_x$ layer. Similar to the finding of Zdenek et al. [16], we find that 1-$R_{PDS}$-$T_{PDS}$ spectrum aligns well with the measured absorption $A_{PDS}$. For the RT measurements, total $R$ and $T$ of symmetric samples were measured using a PerkinElmer Lambda 1050 equipped with an integrating sphere accessory. In the wavelength 300–860 nm, the spectral slit width is 2 nm and the integration time of the photomultiplier tube detector was set to 0.4 s. In the wavelength range of 860–2000 nm, the spectral slit width varies from 5 to 20 nm and it uses InGaAs detector with integration time set to 1 s. The spectrophotometer was calibrated by measuring the reflectance of a calibrated highly reflective reference sample (*Spectralon*) and a dark measurement (i.e. with the light beam blocked). We measured the centre spot of the samples in both reflectance and transmittance measurements. Table 2 gives an overview of the executed measurements and their related samples.

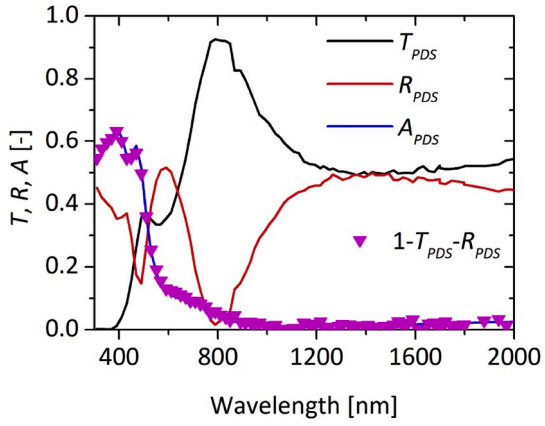


**Fig. 3.** $R_{PDS}$, $T_{PDS}$, and $A_{PDS}$ spectra measured at the same spot of an n-type doped poly-$SiO_x$ layer on quartz substrate. 1-$T_{PDS}$-$R_{PDS}$ and $A_{PDS}$ spectra coincide, even though they come from different detectors for $R_{PDS}$ and $T_{PDS}$ and CCD camera for $A_{PDS}$ [16].

**Table 2**
Samples for PDS, SE, Raman and RT measurements.

| Experiment | Name | Substrate | Type of layer | $d_{layer}$ [nm] | $R_{CO_2}$ or $R_{CH_4}$ or $R_{PH_3}$ or $R_{B_2H_6}$ |
|---|---|---|---|---|---|
| PDS | $R_{CO2}$ | quartz | poly-$SiO_x$ (n) | 100 nm | [0–0.83] |
| | $R_{CH4}$ | quartz | poly-$SiC_x$ (n) | 100 nm | [0.54–0.85] |
| RT | F0 | Flat wafer | – | – | – |
| | F1 | Flat wafer | poly-$SiC_x$ (n) | 30 nm | 0.69 |
| | X0 | Textured wafer | – | – | – |
| | X1 | Textured wafer | poly-$SiC_x$ (n) | 30 nm | 0.69 |
| | X3 | Textured wafer | poly-$SiC_x$ (p) | 30 nm | 0.69 |
| | X1-$R_{PH_3}$ | Textured wafer | poly-$SiC_x$ (n) | 30 nm | [0.13–0.33] |
| | X3-$R_{B_2H_6}$ | Textured wafer | poly-$SiC_x$ (p) | 30 nm | [0.13–0.33] |
| | X2 | Textured wafer | poly-$SiO_x$ (n) | 60 nm | 0.62 |
| | X4 | Textured wafer | Poly-$SiO_x$ (p) | 37 nm | 0.2 |
| | X2-$R_{PH_3}$ | Textured wafer | poly-$SiO_x$ (n) | 40 nm | [0.33–0.83] |
| | X4-$R_{B_2H_6}$ | Textured wafer | poly-$SiO_x$ (p) | 37 nm | [0.11–0.65] |

### 2.3. Optical modelling

The refractive index and absorption coefficients are obtained from ellipsometer using Cody-Lorentz model. As we will show in section 3.1.1, our CSPCs are mixed phase materials, and we considered using Effective Medium Approximation (EMA) but this approach did not improve the fit further. It is possible to add a Drude term to represent FCA, as commonly done for metals [21–23]. However, Drude model possesses several deficiencies [24]. In our samples FCA is relatively weak, adding a Drude term did not lead to satisfactory results. Varying input parameters of Drude model, and therefore varying absorption coefficients at long wavelengths, did not significantly affect the quality of the ellipsometry data fit. This implies that the Drude model, when used for our layers, can give widely different absorption coefficients. As obtained absorption coefficients would not be reliable, the Drude term was not included. GenPro4 is an optical model for simulation of solar cells in which ray optics and wave optics are combined [17]. It is suitable for quickly and accurately simulating c-Si solar cells with multilayer structures [17]. In this study, we have used GenPro4 to simulate the thin films deposited on both sides of textured wafers (see Fig. 1b). The needed absorption coefficients were derived using two methods: the Ritter-Weiser applied on PDS spectra and the IM from RT spectra.

To obtain wavelength-dependent α of flat layers on quartz from PDS, the Ritter-Weiser formula [16] was used:

$$2e^{(ad)} = (1-r)\left(1+\frac{A_{PDS}}{T_{PDS}}\right) + \sqrt{(1-r)^2\left(1+\frac{A_{PDS}}{T_{PDS}}\right)^2 + 4r} \quad (3)$$

where absorptance, transmittance and thickness are denoted by $A$, $T$ and $d$, respectively, and the ratio $r$ is defined as

$$r = \left(\frac{n-m}{n+m}\right)^2 \quad (4)$$

In Equation (4), $n$ and $m$ are the real part of refractive indexes of the layer under test and of the surrounding medium (in our case, FC72), respectively. Wavelength-dependent $n$ and $d$ of the layer were obtained by SE deploying a Cody-Lorentz fitting.

Spitzer et al. provided a detailed physical model for absorption by

free charge carriers, taking into account their interaction with the lattice and impurities [25,26]. The model has been validated for crystalline materials, including c-Si, but it is not directly applicable to the amorphous/crystalline mixed-phase materials like the poly-Si alloys hereby considered [26]. For deriving the absorption coefficient from the absorptance of a layer on textured c-Si substrate, we used the IM approach [19]. This approach is executed using Genpro4 software. For our specific purpose of determining the absorption coefficients of mixed phase materials, the Rudiger model, despite its empirical nature, is an improvement of Schroeder [27] and Green [28] models and therefore is used in this work. Rudiger has given the following equations to calculate the absorption coefficients due to FCA in p-type and n-type highly-doped c-Si, respectively [19]. Here, $p$ and $n$ are the doping concentration:

$$\frac{\alpha_{FC,p}}{cm^{-1}} = 2.6 \times 10^{-18} \times \left(\frac{\lambda}{\mu m}\right)^{2.4} \times \frac{p}{cm^{-3}} \quad (5)$$

$$\frac{\alpha_{FC,n}}{cm^{-1}} = 1.8 \times 10^{-18} \times \left(\frac{\lambda}{\mu m}\right)^{2.6} \times \frac{n}{cm^{-3}} \, . \quad (6)$$

We assume that in the wavelength range from 800 to 2000 nm, the absorption coefficient is due to the FCA ($\alpha_{FC}$), and is given by the following equation [19]:

$$\frac{\alpha_{FC}}{cm^{-1}} = C \times \left(\frac{\lambda}{\mu m}\right)^{x} \quad (7)$$

where constant $C$ and exponent $x$ are fitting parameters. At short wavelengths, these CSPCs layers have high absorption coefficient and the free carriers' contribution is almost negligible. On the other hand, at long wavelengths the FCA starts to play a dominating role. SE is expected to accurately detect the absorption at shorter wavelengths but not the weak absorption at longer wavelengths. Hence, we use the absorption coefficients from SE measurements ($\alpha_e$), combined with those due to FCA accrued from IM approach by choosing accurately $C$ and $x$ in Equation (7) ($\alpha = \alpha_e + \alpha_{FC}$). In this way we are able to get the absorption coefficients in entire wavelength range from 300 to 2000 nm. The input thickness of the layer on textured wafer, that is used for these simulations, is calculated by diving the thickness of layer on flat surface by a factor of 1.7. The contribution of the in-diffused region is relatively small, but the FCA in the in-diffused regions has been incorporated into the model nonetheless. The in-diffused layer has been modelled as a separate layer in the optical model with effective thickness 'd' and uniform doping concentration $C_0$. We choose $C_0$ as the surface concentration, while the effective thickness follows from the following equation [29]:

$$d = \frac{C_n}{C_o} \quad (8)$$

Here $C_n$ is the areal concentration which is calculated by integrating the doping profile in c-Si. The refractive index ('n') for doped Si varies less than 15% due to FCA within the doping range ($10^{15}$ to $10^{21}$ $cm^{-3}$) whereas $\alpha_{FCA}$ varies over several orders of magnitude in the same doping range [30]. Hence, it is safe to assume the refractive index 'n' of intrinsic silicon for our in-diffused layer too. The absorption coefficients ($\alpha$) used for our in-diffused layers are calculated from Rudiger's Equation for highly doped silicon (Equations (5) and (6)) [19]. Fig. 4 shows the measured doping profile of poly-$SiO_x$ layer with in-diffusion in the c-Si bulk. As shown in Fig. 4, $C_0$ is in the order $10^{20}$ $cm^{-3}$ and $C_n$ was derived to be in the order $10^{14}$ $cm^{-2}$. This means that we can model the in-diffused layer as a layer of uniform doping concentration $C_0$ and effective thickness given by Equation (8). Using this approach, the effective thickness comes to be around 10 nm. Similarly, for poly-$SiC_x$ layers, $C_0$ is in the order $10^{17}$ $cm^{-3}$ [6] and $C_n$ was derived to be in the order $10^{11}$ $cm^{-2}$ [6]. Thus the effective thickness comes also to be around 11 nm. The parameters used for modelling the in-diffused region for different CSPCs are given in Table 3.

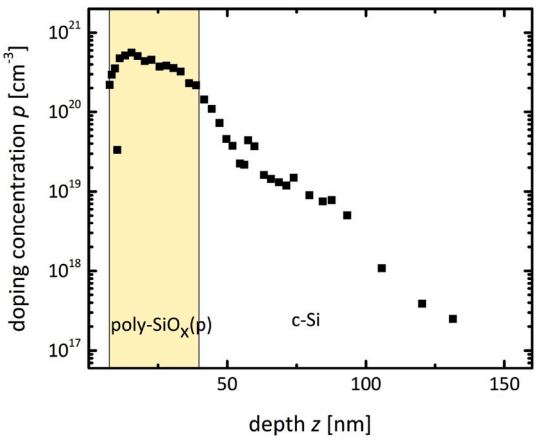


**Fig. 4.** Electrochemical Capacitive-Voltage [ECV] profile of a p-type poly-$SiO_x$ layer on c-Si wafer ($R_{CO2} = 0.2$ and $R_{B2H6} = 0.38$).

**Table 3**
Parameters used for modelling in-diffused region.

| CSPC [source of data] | $C_o$ ($cm^{-3}$) | $C_n$ ($cm^{-2}$) | d (nm) | $\frac{\alpha_{FC}}{cm^{-1}} = C \times \left(\frac{\lambda}{\mu m}\right)^{x}$ |
|---|---|---|---|---|
| n-type doped poly-$SiO_x$ [9] | $3.51 \times 10^{20}$ | $3.63 \times 10^{14}$ | 10.34 | $\frac{\alpha_{FC}}{cm^{-1}} = 631.8 \times \left(\frac{\lambda}{\mu m}\right)^{2.6}$ |
| p-type doped poly-$SiO_x$ [Fig. 4] | $2.15 \times 10^{20}$ | $2.07 \times 10^{14}$ | 9.64 | $\frac{\alpha_{FC}}{cm^{-1}} = 559 \times \left(\frac{\lambda}{\mu m}\right)^{2.4}$ |
| n-type doped poly-$SiC_x$ [6] | $7.24 \times 10^{17}$ | $8.50 \times 10^{11}$ | 11.74 | $\frac{\alpha_{FC}}{cm^{-1}} = 1.30 \times \left(\frac{\lambda}{\mu m}\right)^{2.6}$ |
| p-type doped poly-$SiC_x$ [6] | $7.24 \times 10^{17}$ | $8.50 \times 10^{11}$ | 11.74 | $\frac{\alpha_{FC}}{cm^{-1}} = 1.88 \times \left(\frac{\lambda}{\mu m}\right)^{2.4}$ |

### 2.4. Flowchart for extracting absorption coefficients

In this work, we have used absorption coefficients derived from PDS spectra (flat layers) and verified if they are trustworthy once used to perform optical simulations in GenPro4 software (textured layers). In case the fit was not accurate, we used the IM approach. The followed flowchart is reported in Fig. 5 and can be applied for the extraction of absorption coefficients of other mixed phase materials as well.

## 3. Results

### 3.1. Characterization on quartz substrates

#### 3.1.1. Structural characterization

Raman measurements were performed to understand the structure of our poly-$SiO_x$ and poly-$SiC_x$ layers. Fig. 6a shows the Raman measurements of poly-$SiO_x$ layer with varying $R_{CO2}$. They all show a peak at 517 $cm^{-1}$, which is attributed to phosphorus doped c-Si peak [31]. With increasing $R_{CO2}$, another broad peak centred at 480 $cm^{-1}$ becomes evident. This peak is attributed to the transverse optical mode of amorphous Si [32]. Deconvoluting these spectra, as reported in Fig. 6b for $R_{CO2} = 0.83$ sample, we get also another peak at around 507 $cm^{-1}$, which is attributed to the grain boundary interface between silicon nanocrystals and the surrounding amorphous silicon-oxide matrix [31,33,34]. Our poly-$SiO_x$ layers are therefore mixed phase materials, being formed by a mixture of amorphous and crystalline fractions. As expected, the amorphous silicon-oxide fraction increases with increasing $R_{CO2}$.

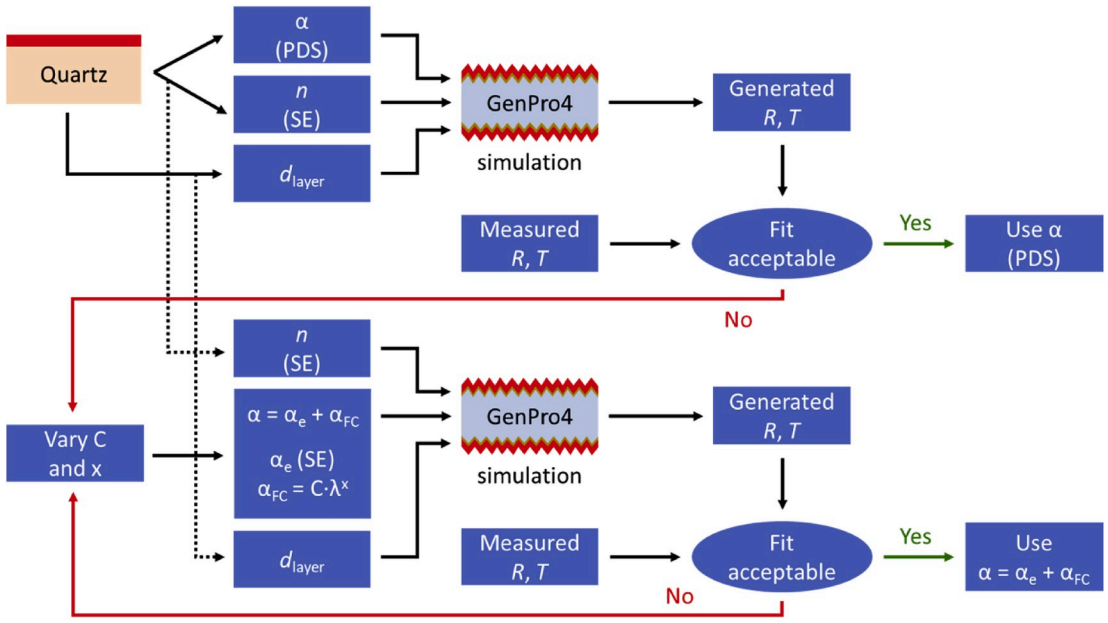


**Fig. 5.** Flowchart for deriving the absorption coefficient of mixed phase materials, where $n$ is the real part of the refractive index; α is the absorption coefficient ($\alpha_e$ and $\alpha_{FC}$ are the SE and IM components, respectively); $d_{layer}$ is the thickness of the layer under test on textured c-Si wafer (calculated by dividing the thickness of layer on flat quartz by 1.7).

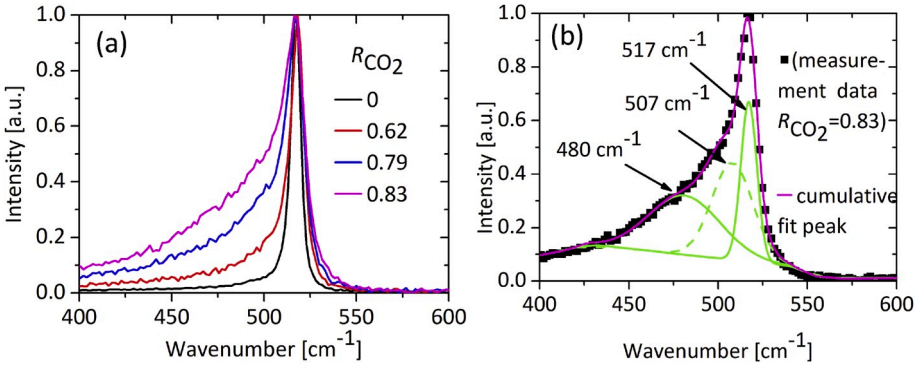


**Fig. 6.** (a) Raman spectra of n-type doped poly-$SiO_x$ layers for different $R_{CO2}$ after annealing; (b) peaks deconvolution reported for the sample with $R_{CO2}$ = 0.83.

Raman measurements performed on the as-deposited and annealed poly-$SiC_x$ layers are included in Fig. 7. A broad peak at around 480 cm$^{-1}$ is observed for the as-deposited samples in Fig. 7a. This peak is attributed to the transverse optical mode of amorphous Si [32]. After annealing, the obtained spectra shown in Fig. 7b are rather different. Along with the amorphous silicon peak, we observe a peak at around 513 cm$^{-1}$. This is quite close to 511 cm$^{-1}$ peak which is attributed to silicon nano-crystals. The downshift of this frequency from 520 cm$^{-1}$ could be due to the compressive stress and grain size related effects [35, 36]. We observe these two peaks only for $R_{CH4}$ = 0.54 and 0.69. This indicates presence of nc-Si grains and reveals that also these layers have a mixed phase structure. For $R_{CH4}$ = 0.85, we observe only a broad peak

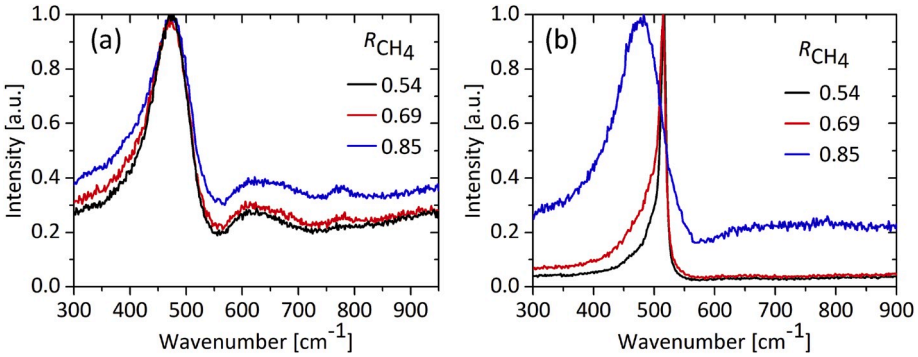


**Fig. 7.** Raman measurements of n-type doped poly-$SiC_x$ with varying $R_{CH4}$ for (a) as deposited layers (b) annealed layers.

at around 480 $cm^{-1}$ indicating its completely amorphous phase.

### 3.1.2. Real part of refractive index

SE measurements reported in Fig. 8a and b shows the real part of the refractive index of our poly-$SiO_x$ and poly-$SiC_x$ layers, respectively, with intrinsic hydrogenated amorphous silicon (a-Si:H) and n-type c-Si as references. In general, from c-Si reference to poly-$SiO_x$ and poly-$SiC_x$ layers, we see two trends: (i) a decrease of peak value and (ii) a peak shift towards higher wavelengths for increasing $R_{CO2}$ and $R_{CH4}$, respectively. We find that $n$ obtained for poly-$SiO_x$ layers decreases with increasing $R_{CO2}$ in the entire wavelength range from 300 to 2000 nm. For poly-Si ($R_{CO2} = 0$) layer, as expected, $n$ is quite similar to that of n-type c-Si. We also observe that, as the $R_{CO2}$ increases, the peak value of $n$ decreases down to 3.9, approaching the value of 2.85 for longer wavelengths. The decrease in peak value of $n$ is another indication that our poly-$SiO_x$ becomes more amorphous with increasing $R_{CO2}$, as supported by Raman measurements (see Fig. 6a). Similarly, for n-type doped poly-$SiC_x$ layers, the peak value of $n$ decreases with increasing $R_{CH4}$, even though already for wavelengths longer than 800 nm all trends are closely bundled (see Fig. 8b).

### 3.1.3. Absorption coefficients from PDS

Fig. 9a and b shows the absorption coefficients of n-type doped poly-$SiO_x$ and poly-$SiC_x$ layers respectively from PDS measurements. In both cases, we used a-Si and n-type doped c-Si ($10^{20}$ $cm^{-3}$ and $10^{21}$ $cm^{-3}$ doping concentrations) as references. The absorption coefficients of n-type doped c-Si with doping concentrations $10^{20}$ $cm^{-3}$ and $10^{21}$ $cm^{-3}$ have been generated using equations (5) and (6) [19]. Our poly-$SiO_x$ layers, being partly amorphous and party crystalline as previously shown by Raman measurements, are less absorptive than a-Si and more absorptive than c-Si in the visible region. At longer wavelengths, the absorption coefficients of poly-$SiO_x$ layers are within the reference lines of doped c-Si. This indicates that our layers have doping concentration in the range between $10^{20}$ $cm^{-3}$ and $10^{21}$ $cm^{-3}$. We observe that by increasing $R_{CO2}$, the absorption coefficient increases in the visible region but decreases in the near infrared region. In other words, poly-$SiO_x$ layers absorb more than poly-Si ($R_{CO2} = 0$) in the visible region, while they are more transparent in the near infrared region with increasing $R_{CO2}$. For poly-$SiC_x$ layers, the absorption coefficients increase for increasing $R_{CH4}$ in the visible and near infrared region (see Fig. 9b). In other words, poly-$SiC_x$ layers tend to absorb more in the visible and near infrared region as $R_{CH4}$ increases. To describe this phenomenon further investigation is needed.

## 3.2. RT measurements on c-Si substrate

### 3.2.1. Flat versus textured c-Si wafer substrates

Fig. 10a shows wavelength-dependent $R$ and $T$ spectra of flat samples, a bare c-Si wafer (F0) and a c-Si wafer double-side coated with 30-nm thick layers of poly-$SiC_x$ (F1). Note that in all cases 1-$R$ and $T$ are plotted, so that one can observe the absorptance $A$ directly from the graph in terms of $(1 - R) - T$. As expected, below 900 nm wavelength the c-Si wafer is opaque ($T = 0$). Beyond 1200 nm, c-Si is known to have a low absorption coefficient and the flat c-Si wafer hardly absorbs any light ($A \approx 0$). Sample F1 also has a low absorptance for wavelengths larger than 1200 nm. If we derive absorption coefficients from this value, the error margin will be large due to the weakness of the absorptance compared to the measurement error. This is the limitation in obtaining the absorption coefficient of weakly absorbing films from RT measurements, at least for flat samples.

Next, referring to Table 2, the textured samples X0 to X1 are considered, whose measured 1-$R$ and $T$ spectra are shown in Fig. 10b. The grey symbols show the results of sample X0, the bare double-side textured wafer. Here, we focus on the absorptance for wavelengths longer than 1200 nm. Due to light trapping, texturing has amplified the long-wavelength absorptance in the c-Si wafer, corresponding to an increase in path length of light [37]. The blue symbols show the measured spectra of double-side textured sample X1 symmetrically coated with 30-nm thick poly-$SiC_x$ layers. Compared to sample F1, the absorptance is now increased. This suggests that the texture not only enhances the absorptance in the c-Si wafer, but also that of the thin film deposited on top of the surface textures. Similarly, RT measurements were performed on sample X2 (double-side textured wafer symmetrically coated with 60-nm thick poly-$SiO_x$ layers). The corresponding measurement results are shown in Fig. 11a. The results above indicate that using symmetric, double-side textured wafers, the weak absorption of light at wavelength longer than 1200 nm could be successfully amplified and detected with RT measurements.

### 3.2.2. Verifying PDS absorption coefficients

To verify if the absorption coefficients obtained from PDS of n-type doped poly-$SiO_x$ and poly-$SiC_x$ layers can be used for optical modelling, we have performed simulations using GenPro4. The structure simulated has the thin film layer structure (poly-$SiO_x$ or poly-$SiC_x$) deposited on both sides of the textured wafer, as shown in Fig. 1b. The optical model also incorporates 1.5-nm thick NAOS-based tunnelling $SiO_2$. These simulations use α obtained from PDS and $n$ from ellipsometer as input to generate $R$ and $T$ spectra. The input thickness of the layer on textured wafer is calculated by dividing the layer's thickness on flat surface by a factor of 1.7. For thickness values used in optical simulations refer to Table 2. Generated $R$ and $T$ spectra have been compared with their measured counterparts as shown in Fig. 11a and b for sample X2 and X1, respectively. The corresponding absorptance and absorption coefficients of poly-$SiO_x$ and poly-$SiC_x$ layers are shown in Fig. 12a and b, respectively. A similar analysis has been done for p-type doped poly-$SiO_x$ and poly-$SiC_x$ layers (see Fig. 13a and Fig. 13b).

We observe that the generated curves fit the measured curves quite well from 400 nm to 1200 nm. In the wavelength range between 300 and

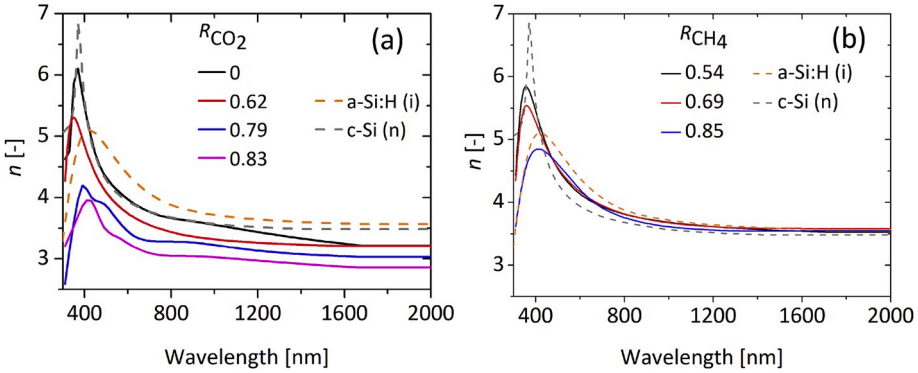


**Fig. 8.** Refractive indices of n-type doped (a) poly-$SiO_x$ or (b) poly-$SiC_x$ layers with varying $R_{CO2}$ or $R_{CH4}$, respectively.

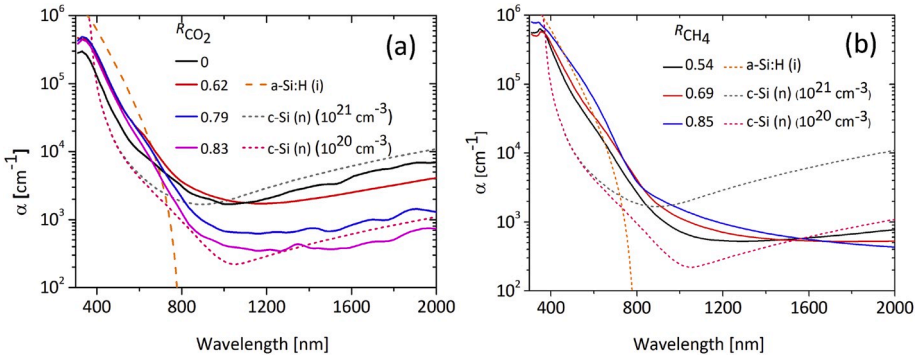


**Fig. 9.** Absorption coefficients from PDS measurements of n-type doped (a) poly-$SiO_x$ and (b) poly-$SiC_x$ layers with varying $R_{CO2}$ and $R_{CH4}$, respectively. Intrinsic amorphous silicon and c-Si (characterized by two different doping concentrations) were used as reference.

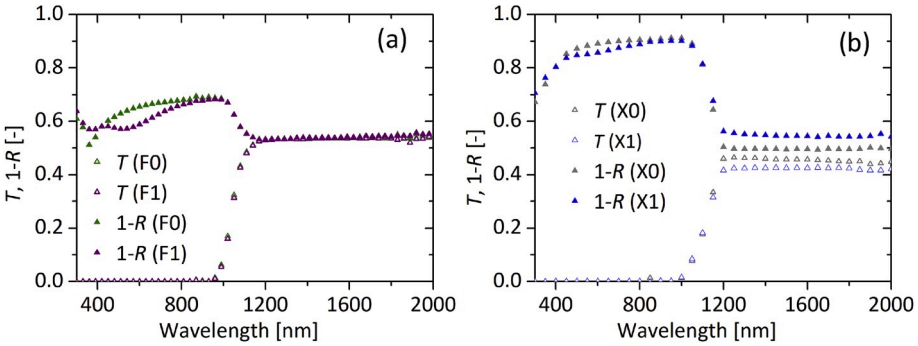


**Fig. 10.** Wavelength-dependent spectra from RT measurements (1-*R* and *T*) of (a) F0 and F1 samples and (b) X0 and X1 samples. For a description of the samples, refer to Table 2.

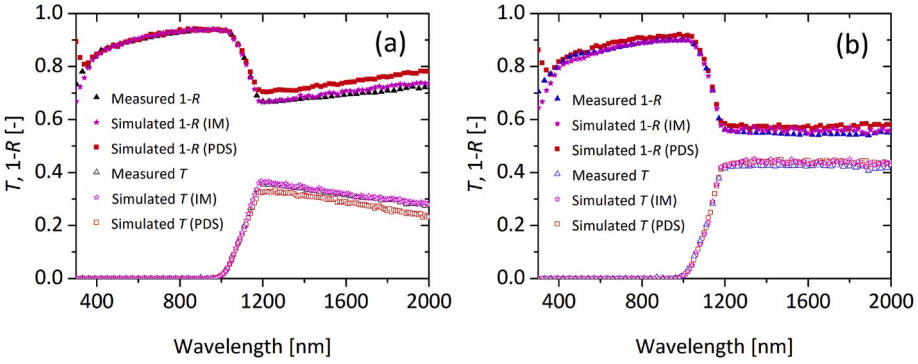


**Fig. 11.** GenPro4 simulation results using optical properties from PDS or IM approach compared to measured 1-*R* and *T* spectra measurements for (a) X2 and (b) X1 samples. For a description of the samples, refer to Table 2.

400 nm, the curves do not fit for poly-$SiO_x$ and poly-$SiC_x$ layers due to their transmittance being below 1%. This is the case of our CSPCs under test. Also, for wavelengths longer than 1200 nm, we do not observe an accurate fit in case of poly-$SiO_x$ and poly-$SiC_x$ layer. Referring to the flowchart in Fig. 5, we passed to the IM approach for extracting α directly from RT measurements.

### 3.2.3. *Inverse modelling (IM) approach*

Choosing values of C and x in Equation (7), FCA coefficients can be derived for the CSPCs under test. The fit of the bare textured sample X0 yields C = 0.025 and x = 2.0. These values for the c-Si bulk absorption coefficient are then also used in all subsequent IM simulations. In case of sample X2, textured symmetrical 60-nm thick n-type doped poly-$SiO_x$ layer on c-Si wafer, the fit yields C = 840 and x = 1.65. With respect to the simulated *R* and *T* spectra based on α from PDS, there is now a very good agreement measured spectra (see Fig. 11a). In case of X1 sample, textured symmetrical 30-nm thick n-type doped poly-$SiC_x$ layer on c-Si wafer, the fit yields C = 650 and x = -0.8, which result in even closer agreement between simulated and measured spectra (see Fig. 11b). In case of the X4 sample, a textured symmetrical 37-nm thick p-type doped poly-$SiO_x$ layer on c-Si wafer, the fit yields C = 4200 and x = 0.5 (see Fig. 13a). For X3 sample, a textured symmetrical 30-nm thick p-type doped poly-$SiC_x$ layer on c-Si wafer, C = 1290 and x = -2.5 give a close agreement between measured and simulated absorptance spectra (see Fig. 13b).

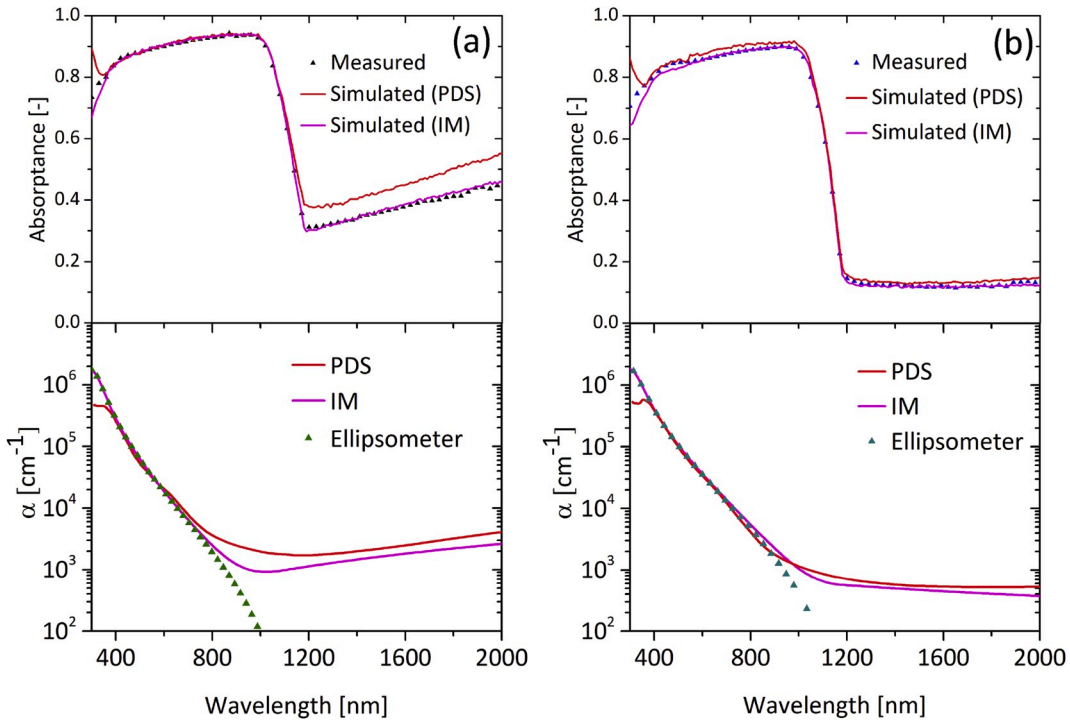


**Fig. 12.** Top panels: overall absorptance in n-type doped layer /textured c-Si substrate symmetric samples; bottom panels: absorption coefficient of the CSPC layer under test. (a) Poly-$SiO_x$ ($R_{CO2} = 0.62$); (b) poly-$SiC_x$ ($R_{CH4} = 0.69$).

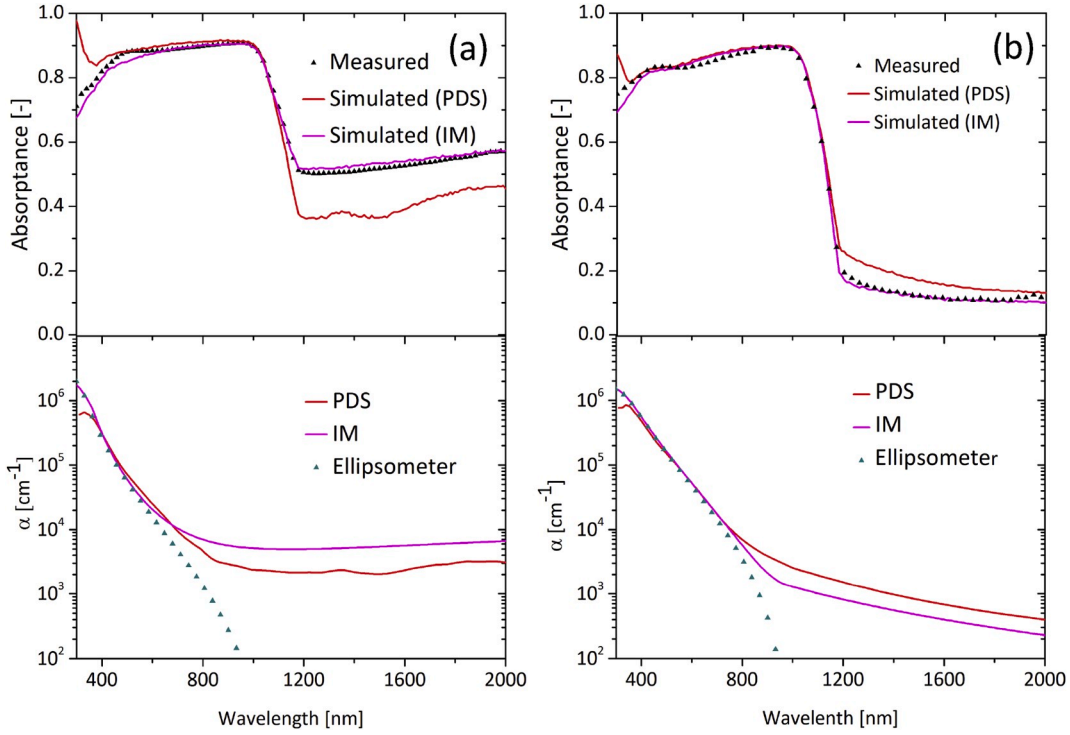


**Fig. 13.** Top panels: overall absorptance in p-type doped layer /textured c-Si substrate symmetric samples; bottom panels: absorption coefficient of the CSPC layer under test. (a) Poly-$SiO_x$ ($R_{CO2} = 0.2$); (b) poly-$SiC_x$ ($R_{CH4} = 0.69$).

## 4. Discussion

### 4.1. Absorption coefficients

The obtained α from both PDS and IM approaches of some n-type CSPCs layers under test (X2 and X1) are shown in the bottom panels of Fig. 12a and b, respectively. In the same Figures, we report also the absorptance spectra, which include both contributions of the bulk c-Si wafer and of the layers sandwiching it. For n-type doped poly-$SiO_x$ layers, we get a fit with an average deviation of 4.3% and 0.7% from PDS

and IM approaches, respectively. For n-type doped poly-$SiC_x$ layers, we get a fit with an average deviation of 1.6 % and 0.8% from PDS and IM techniques respectively. The obtained α, also from both PDS and IM approaches, of p-type CSPCs layers under test (X4 and X3) are shown in the bottom panels of Fig. 13a and b, respectively. In the same Figures, the absorptance spectra are also reported. For p-type doped poly-$SiO_x$ layer, we get an average deviation of 7.6% and 1.1% for PDS and IM approaches, respectively. For p-type doped poly-$SiC_x$ layer, we get an average deviation of 2.9% and 1% for PDS and IM approaches, respectively.

We find that these absorption coefficients successfully estimate FCA in the wavelength range above 800 nm, which ellipsometer is unable to detect. While the PDS approach proves to be straightforward with regards to sample preparation, the IM approach ultimately shows a better fit for optical modelling of CSPCs on c-Si substrate. Thus, α from IM approach can be used as an input for optical modelling of solar cells endowed with poly-$SiO_x$ and poly-$SiC_x$ CSPCs. In this way, parasitic losses will be better quantified and both single- and multi-junction solar cells will be further improved.

We observe that the absorption coefficients obtained from both techniques have differences especially in the UV and IR part of the spectrum. This is ascribed to the likely difference in growth and subsequent crystallization of the layers under test on the different substrates used in these two methods. By obtaining absorption coefficients from PDS and IM techniques independently, we could compare the optical behaviour of the layer on both quartz and c-Si substrates. Using the advantages of both the techniques, accurate absorption coefficients for optical modelling can be obtained in the wavelength range from 300 to 2000 nm for both poly-$SiO_x$ and poly-$SiC_x$ layers either on quartz or on textured c-Si wafer. PDS can be used to measure absolute absorption directly. Using this technique, the absorption coefficients can be derived as discussed in sections 2.3 and 2.4. However, its limitation is that it does not predict correct absorption when the transmittance is below 1%. On the other hand, the IM approach helps in getting data at long wavelengths for CSPCs in solar cells. This approach depends on the absorption coefficients from SE in the UV/visible range but adds the FCA component, which starts to play a role for wavelength longer than 800 nm.

### 4.2. Effect of $R_{CO2}$, $R_{CH4}$, $R_{PH_3}$ and $R_{B_2H_6}$ on optical properties

The poly-$SiO_x$ and poly-$SiC_x$ CSPCs are mixed phase materials and, by varying, respectively, $R_{CO2}$ and $R_{CH4}$, their optical properties can be altered. We observe that their $n$ decreases with increasing $R_{CO2}$ or $R_{CH4}$ [6]. Thus, $n$ can be somewhat tuned to minimize front reflection in FBC cells endowed with these CSPCs. We also note that FCA decreases for n-type doped poly-$SiO_x$ layers in the infrared region with respect to the reference poly-Si ($R_{CO2} = 0$). The reference poly-Si ($R_{CO2} = 0$) can be found in Ref. [5]. The probable reason could be that, with increasing $R_{CO2}$, the a-$SiO_x$ phase in the poly-$SiO_x$ layer is expected to increase, as supported by Raman measurements (see Fig. 4a). Since the doping efficiency of the crystalline phase is higher than that of the amorphous phase [38], the incorporation of the dopants into the a-$SiO_x$ phase is more difficult, thereby decreasing FCA for increasing $R_{CO2}$.

Fig. 14a and b shows the analysis of additional samples for n-type doped poly-$SiO_x$ and p-type doped poly-$SiO_x$ layers using IM analysis with different $R_{PH_3}$ and $R_{B_2H_6}$, respectively. A similar analysis is shown for n-type and p-type doped poly-$SiC_x$ layers in Fig. 15a and b, respectively. Samples with ratio $R_{PH_3} = 0.54$ (Fig. 14a) and $R_{PH_3} = 0.13$ (Fig. 15a) are the reference samples used in Fig. 12a and b, respectively. Similarly, samples with ratio $R_{B_2H_6} = 0.38$ (Fig. 14b) and $R_{B_2H_6} = 0.13$ (Fig. 15b) are the reference samples shown in Fig. 13a and b, respectively. As expected, we find that with the increase in doping gas flow ratio, the FCA increases. In these cases, our IM approach not only proves to be effective with regards to textured CSPC layers, but also to carry out the expected trend.

### 4.3. Effect of thickness on absorption coefficients extracted by IM

We performed additional experiments, in which we have deposited different thickness of p-type doped poly-$SiO_x$ layer ($R_{CO_2} = 0.2$ and $R_{B_2H_6} = 0.38$ ). A fixed absorption coefficient obtained from inverse modelling approach (as shown in Fig. 13a) of p-type doped poly-$SiO_x$ layer has been used. The simulated absorptance of this layer deposited on both sides of double side textured wafer for thickness values of 10 nm, 15 nm and 37 nm is shown in Fig. 16a and confirms that the thicker the layer is, the higher the absorptance is. With only one refractive index and absorption coefficient data sets, we managed to get a very good fit with an average deviation of only 1%, 0.8% and 1.2% for samples with thickness of 10 nm, 15 nm and 37 nm, respectively. A similar analysis was done for p-type doped poly-$SiC_x$ layer ($R_{CH_4} = 0.69$ and $R_{B_2H_6} = 0.13$). Using the absorption coefficient of this p-type doped poly-$SiC_x$ layer (as shown in Fig. 13b), we measured and simulated the total absorptance in layers deposited on both sides of double side textured wafer for different thicknesses. The results are shown in Fig. 16b, where we demonstrate an average deviation of 1%, 0.6% and 1.2% for samples with thickness 30 nm, 51 nm and 90 nm, respectively. Again, this shows that the absorption coefficient obtained from IM approach for a single layer thickness can be used to simulate absorptance of layers of different thicknesses.

## 5. Conclusions

Weak FCA at long wavelengths is difficult to detect using SE. In this study, we demonstrated that, from PDS or IM approach, we could successfully extract the absorption coefficients of n-type and p-type doped poly-$SiO_x$ and poly-$SiC_x$ layers on fused silica quartz substrate and on textured c-Si wafer substrate, respectively, in the extended wavelength range from 300 to 2000 nm. The absorption coefficients of n-type and p-type doped poly-$SiO_x$ and poly-$SiC_x$ layers obtained from PDS and IM

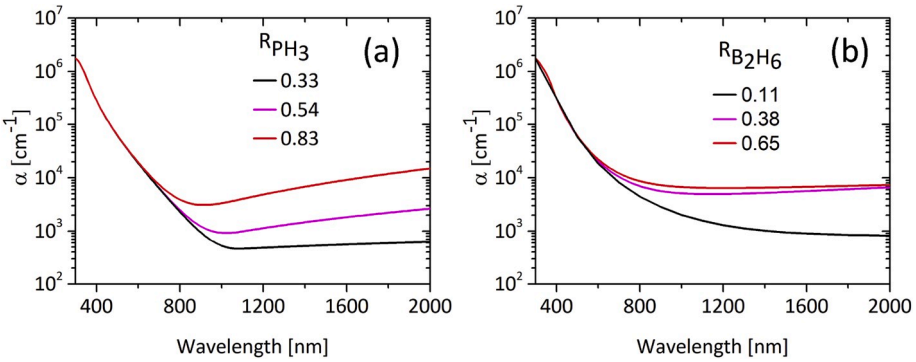


**Fig. 14.** Variation of absorption coefficients with changing $R_{PH_3}$ and $R_{B_2H_6}$ of (a) n-type doped poly-$SiO_x$ ($R_{CO2} = 0.62$); (b) p-type doped poly-$SiO_x$ ($R_{CH4} = 0.2$).

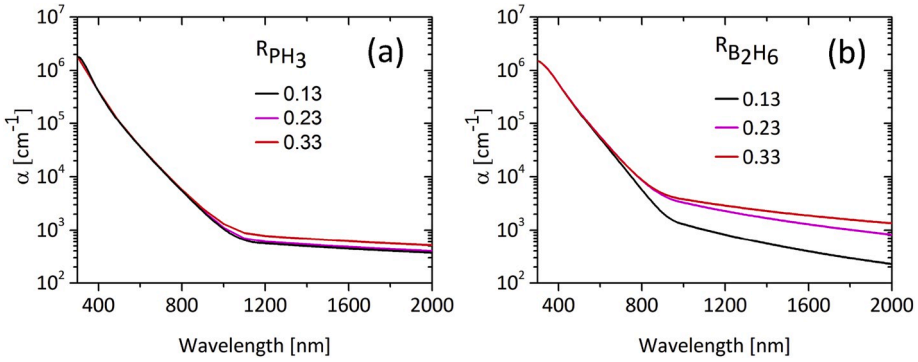


**Fig. 15.** Variation of absorption coefficients with changing $R_{PH_3}$ and $R_{B_2H_6}$ of (a) n-type doped poly-SiC$_x$ ($R_{CO2} = 0.69$); (b) p-type doped poly-SiC$_x$ ($R_{CH4} = 0.69$).

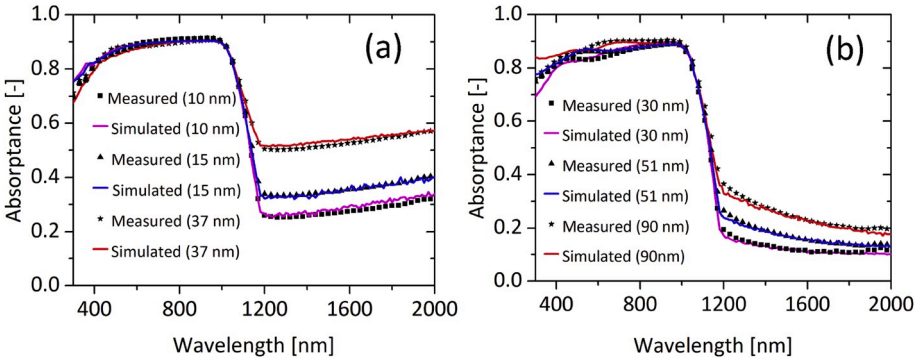


**Fig. 16.** Measured and simulated overall absorptance in p-type doped layer /textured c-Si substrate symmetric samples (a) p-type doped poly-SiO$_x$ ($R_{CO2} = 0.2$ and $R_{B_2H_6} = 0.38$); (b) p-type doped poly-SiC$_x$ ($R_{CH4} = 0.69$ and $R_{B_2H_6} = 0.13$).

approach have differences. These most likely stem from the different substrates used in these two techniques. By using the RT measurement technique on double-side textured samples, we could successfully measure the weak FCA in our CSPCs layers. Using the absorption coefficients from the IM approach, we got a good fit (around or less than 1% average deviation) between measured and simulated $R$ and $T$ spectra. Obtained α can now be used as an input to study the optical behaviour of single- and multi-junction solar cells endowed with poly-SiO$_x$ and poly-SiC$_x$ CSPCs. We also analysed that by changing the $R_{CO2}$ and $R_{CH4}$, the optical properties of poly-SiO$_x$ and poly-SiC$_x$ layers can be altered. With increase in $R_{PH3}$ and $R_{B2H6}$, FCA increases in our CSPCS.

## Declaration of competing interest

The authors declare that they have no known competing financial interests or personal relationships that could have appeared to influence the work reported in this paper.

## CRediT authorship contribution statement

**M. Singh:** Writing - original draft, Formal analysis, Data curation, Investigation. **R. Santbergen:** Methodology, Supervision, Writing - original draft. **L. Mazzarella:** Investigation. **A. Madrampazakis:** Investigation. **G. Yang:** Investigation. **R. Vismara:** Resources. **Z. Remes:** Resources. **A. Weeber:** Supervision, Funding acquisition. **M. Zeman:** Supervision, Funding acquisition. **O. Isabella:** Supervision, Writing - original draft, Visualization.

## Acknowledgements

The authors would like to thank NWO JSP III (680-91-011) program for financial support. The authors would also like to thank Martin Lendinsky and Antonin Fejfar for helping in the PDS measurements.

## Appendix A. Supplementary data

Supplementary data to this article can be found online at https://doi.org/10.1016/j.solmat.2020.110507.

## References

[1] G. Yang, A. Ingenito, N. van Hameren, O. Isabella, M. Zeman, Design and application of ion- implanted polySi passivating contacts for interdigitated back contact c-Si solar cells, Appl. Phys. Lett. 108 (3) (2016), 033903.
[2] G. Yang, A. Ingenito, O. Isabella, M. Zeman, IBC c-Si solar cells based on ion-implanted poly- silicon passivating contacts, Sol. Energy Mater. Sol. Cell. 158 (2016) 84–90.
[3] F. Feldmann, C. Reichel, R. Müller, M. Hermle, The application of poly-Si/SiOx contacts as passivated top/rear contacts in Si solar cells, Sol. Energy Mater. Sol. Cell. 159 (2017) 265–271.
[4] A. Richter, J. Benick, F. Feldmann, A. Fell, M. Hermle, S. Glunz, n-Type Si solar cells with passivating electron contact: identifying sources for efficiency limitations by wafer thickness and resistivity variation, Sol. Energy Mater. Sol. Cell. 173 (2017) 96–105.
[5] G. Yang, P. Guo, P. Procel, A. Weeber, O. Isabella, M. Zeman, Poly-crystalline silicon-oxide films as carrier-selective passivating contacts for c-Si solar cells, Appl. Phys. Lett. 112 (19) (2018), 193904.
[6] A. Ingenito, G. Nogay, J. Stuckelberger, P. Wyss, L. Gnocchi, C. Allebe, et al., Phosphorous-doped silicon carbide as front-side full-area passivating contact for double-side contacted c-Si solar cells, IEEE J. Photovolt. 9 (2) (2018) 346–354.
[7] G. Yang, Y. Zhang, P. Procel, A. Weeber, O. Isabella, M. Zeman, Poly-Si(O)x passivating contacts for high-efficiency c-Si IBC solar cells, Energy Procedia 124 (2017) 392–399.
[8] J. Stuckelberger, G. Nogay, P. Wyss, A. Ingenito, C. Allebe, J. Horzel, et al., Recombination analysis of phosphorus-doped nanostructured silicon oxide passivating electron contacts for silicon solar cells, IEEE J. Photovolt. 8 (2) (2018) 389–396.
[9] J. Stuckelberger, G. Nogay, P. Wyss, Q. Jeangros, C. Allebé, F. Debrot, et al., Passivating electron contact based on highly crystalline nanostructured silicon oxide layers for silicon solar cells, Sol. Energy Mater. Sol. Cell. 158 (2016) 2–10.
[10] O. Isabella, G. Yang, G. Limodio, P. Procel, M. Singh, Y. Zhao, A. Weeber, M. Zeman, Fully-passivated, Black, High-Efficiency C-Si Solar Cells Featuring Passivating Contacts, Silicon PV, Leuven, Belgium, 2019.

[11] G. Nogay, A. Ingenito, E. Rucavado, Q. Jeangros, J. Stuckelberger, P. Wyss, et al., Crystalline silicon solar cells with coannealed electron- and hole-selective SiCx passivating contacts, IEEE J. Photovolt. 8 (6) (2018) 1478–1485.
[12] F. Iacona, C. Bongiorno, C. Spinella, S. Boninelli, F. Priolo, Formation and evolution of luminescent Si nanoclusters produced by thermal annealing of SiOx films, J. Appl. Phys. 95 (7) (2004) 3723–3732.
[13] I. Mack, J. Stuckelberger, P. Wyss, G. Nogay, Q. Jeangros, J. Horzel, et al., Properties of mixed phase silicon-oxide-based passivating contacts for silicon solar cells, Sol. Energy Mater. Sol. Cell. 181 (2018) 9–14.
[14] G. Nogay, J. Stuckelberger, P. Wyss, Q. Jeangros, C. Allebé, X. Niquille, et al., Silicon-Rich silicon carbide hole-selective rear contacts for crystalline-silicon-based solar cells, ACS Appl. Mater. Interfaces 8 (51) (2016) 35660–35667.
[15] H. Fujiwara, Spectroscopic Ellipsometry: Principles and Applications, Wiley, Chichester, 2007.
[16] Z. Remes, R. Vasudevan, K. Jarolimek, A.H. Smets, M. Zeman, The optical spectra of a-Si:H and a-SiC:H thin films measured by the absolute photothermal deflection spectroscopy (PDS), Solid State Phenom. 213 (2014) 19–28.
[17] R. Santbergen, T. Meguro, T. Suezaki, G. Koizumi, K. Yamamoto, M. Zeman, GenPro4 optical model for solar cell simulation and its application to multijunction solar cells, IEEE J. of Photovolt. 7 (3) (2017) 919–926.
[18] E. Yablonovitch, Statistical ray optics, J. Opt. Soc. Am. 72 (7) (1982) 899–907.
[19] M. Rudiger, J. Greulich, A. Richter, M. Hermle, Parameterization of free carrier absorption in highly doped silicon for solar cells, IEEE Trans. Electron. Dev. 60 (7) (2013) 2156–2163.
[20] C. Pahud, O. Isabella, A. Naqavi, F.-J. Haug, M. Zeman, H.P. Herzig, et al., Plasmonic silicon solar cells: impact of material quality and geometry, Optic Express 21 (105) (2013) A786–A797.
[21] M. Dressel, M. Scheffler, Verifying the Drude response, Ann. Phys. 15 (2006) 535–544.
[22] S. Roberts, Optical properties of Nickel and Tungsten and their interpretation according to Drude's formula, Phys. Rev. 114 (1) (1959) 104.
[23] S. Roberts, Interpretation of the optical properties of metal surfaces, Phys. Rev. 100 (6) (1955) 1667.
[24] A.F. Gibson, Infra-red and microwave modulation using free carriers in semiconductors, J. Sci. Instrum. 35 (8) (1958) 273.
[25] H.Y. Fan, W. Spitzer, R.J. Collins, Infrared absorption in n-type germanium, Phys. Rev. 101 (2) (1956) 566.
[26] W. Spitzer, H.Y. Fan, Infrared absorption in n-type silicon, Phys. Rev. 108 (2) (1957) 268.
[27] D.K. Schroder, R.N. Thomas, J.C. Swartz, Free carrier absorption in silicon, IEEE J. Solid State Circ. 13 (1) (1978) 180–187.
[28] M.A. Green, Silicon Solar Cells: Advanced Principles and Practice, University of New South Wales, Sydney, Australia, 1995, p. 48.
[29] R. Santbergen, R.J.C. van Zolingen, The absorption factor of crystalline silicon PV cells: a numerical and experimental study, Sol. Energy Mater. Sol. Cell. 92 (4) (2008) 432–444.
[30] J. Isenberg, W. Warta, Free carrier absorption in heavily doped silicon layers, Apl. Phys. Lett. 84 (13) (2004) 2265–2267.
[31] T.C.-J. Yang, K. Nomoto, B. Puthen-Veettil, Z. Lin, L. Wu, T. Zhang, et al., Properties of silicon nanocrystals with boron and phosphorus doping fabricated via silicon rich oxide and silicon dioxide bilayers, Mater. Res. Express 4 (7) (2017), 075004.
[32] M. Marinov, N. Zotov, Model investigation of the Raman spectra of amorphous silicon, Phys. Rev. B 55 (5) (1997) 2938–2944.
[33] J. Wei, A. Wirth, M.C. Downer, B.S. Mendoza, Second-harmonic and linear optical spectroscopic study of silicon nanocrystals embedded in $SiO_2$, Phys. Rev. B 84 (16) (2011), 165316.
[34] Q. Cheng, S. Xu, K.K. Ostrikov, Single-step, rapid low-temperature synthesis of Si quantum dots embedded in an amorphous SiC matrix in high-density reactive plasmas, Acta Mater. 58 (2) (2010) 560–569.
[35] S. Veprek, F.-A. Sarott, Z. Iqbal, Effect of grain boundaries on the Raman spectra, optical absorption, and elastic light scattering in nanometer-sized crystalline silicon, Phys. Rev. B 36 (6) (1987) 3344–3350.
[36] C. Ossadnik, S. Veprek, I. Gregora, Applicability of Raman scattering for the characterization of nanocrystalline silicon, Thin Solid Films 337 (1999) 148–151.
[37] T. Tiedje, E. Yablonovitch, G. Cody, B. Brooks, Limiting efficiency of silicon solar cells, IEEE Trans. Electron. Dev. 31 (5) (1984) 711–716.
[38] A. Lambertz, T. Grundler, F. Finger, Hydrogenated amorphous silicon oxide containing a microcrystalline silicon phase and usage as an intermediate reflector in thin-film silicon solar cells, J. Appl. Phys. 109 (11) (2011), 113109.